Electrical Power and Energy Systems 107 (2019) 680–689

Contents lists available at ScienceDirect

Electrical Power and Energy Systems

journal homepage: www.elsevier.com/locate/ijepes

Linear/quadratic programming-based optimal power flow using linear power flow and absolute loss approximations

P. Fortenbacher*, T. Demiray

Research Center for Energy Networks (FEN), ETH Zurich, Sonneggstrasse 28, 8092 Zurich, Switzerland

ARTICLE INFO

Keywords:
Optimal power flow
Linear/quadratic programming
Power flow approximation

ABSTRACT

This paper presents novel methods to approximate the nonlinear AC optimal power flow (OPF) into tractable linear/quadratic programming (LP/QP) based OPF problems that can be used for power system planning and operation. We consider a linear power flow and branch flow approximation and derive a power loss approximation in the form of absolute value functions that are suitable to cover a broader operating range. The key ideas are (1) to capture power losses and power flows in the full decision variable domain, (2) to combine these approximations to recast the nonlinear constraints of the OPF problem into linear ones, and (3) to solve the approximate OPF problem with off-the-shelf solvers in a non-iterative fashion. In this way, the problem complexity can be reduced significantly. In detail, we present four OPF approximation methods, in which we relax the absolute power loss functions as linear constraints. In a comprehensive case study the usefulness of our OPF methods is analyzed and compared with an existing OPF relaxation and approximation method. As a result, the errors on voltage magnitudes and angles are reasonable, while obtaining near-optimal results for typical scenarios. We find that our methods reduce significantly the computational complexity compared to the nonlinear AC-OPF making them a good choice for power system planning purposes.

1. Introduction

1.1. Motivation

Optimal Power Flow (OPF) is indispensable for current research in power system operation and planning. OPF is widely used in planning problems, or to find optimal generation schedules in active and reactive power at operational level that minimize operational system costs subject to grid constraints.

In both domains, for planning and operation, it is crucial to find tractable formulations of the OPF problems, as they are often intertemporal coupled in the form of multi-period OPF problems. In addition, in combination with long time horizons that are typical for planning problems and large grids, these problems result often in large-scale OPF problems. To manage the complexity to a reasonable level, research has focused on following solution techniques: (1) problem relaxation [1,2] or approximation [3–8], (2) problem decomposition [7,8], and (3) high-performance nonlinear large-scale problem solving [9–12].

Moreover, the combination of the nonlinear power flow equations with binary placement or operational constraints makes these problems even harder to solve. One way to solve such problems is to use mixed-integer programming (MIP) solvers, but those require to rely on (1) problem relaxation or approximation. Therefore, current planning methods include either the well-known lossless DC power flow approximation [13], a lossless approximation of the power flow in the full decision variable domain (active and reactive power, voltage magnitudes and angles) [5] or a power flow representation that does not operate in the full decision variable domain [3,4]. This can result in near-optimal or infeasible solutions, when neither network losses nor the full solution space are considered.

On operational level unit commitment (UC) problems can also be regarded as multi-period OPF problems and use binary decisions to incorporate e.g. generators startup costs. The works [6,7,14] include also the DC power flow approximation which explains why UC problems need to be divided into several stages. E.g. the work [14] accounts for the binary decisions in the first stage, using a linear DC approximation, and then use the nonlinear OPF in the following stages at the cost of optimality, and/or computation time.

As another option relaxing large-scale OPF problems into a second order cone (SOC) programming problem [1] or into an semidefinite programming (SDP) problem [2] could be more accurate, but it is still a complex optimization problem. Consequently, linear approximations are often the first choice to deal with the complexity issue.

* Corresponding author.
E-mail addresses: fortenbacher@fen.ethz.ch (P. Fortenbacher), demirayt@fen.ethz.ch (T. Demiray).

https://doi.org/10.1016/j.ijepes.2018.12.008
Received 17 August 2018; Received in revised form 14 October 2018; Accepted 2 December 2018
0142-0615/ © 2018 Elsevier Ltd. All rights reserved.

Nomenclature

Δv_d	magnitude difference design parameter
$\Delta\theta_d$	angular difference design parameter
$\Delta\boldsymbol{\theta}$, $\Delta\boldsymbol{v}$	decision vector voltage angles and magnitudes
ϵ_θ, ϵ_v	RMS errors on voltage angles and magnitudes
$\epsilon_{\Delta\theta}$, $\epsilon_{\Delta v}$	RMS errors on voltage angle and magnitude differences
θ_s	transformer shift angle
$\theta_k \in \boldsymbol{\theta}$	decision vector voltage angles
$\boldsymbol{a}_q \in \boldsymbol{A}_q$	polygon shape parameters
$\boldsymbol{b}_\theta$, $\boldsymbol{b}_v$	binary decision vector associated with $\Delta\boldsymbol{\theta}$, $\Delta\boldsymbol{v}$
$\boldsymbol{C}_{br}$	branch-node incidence matrix
$\boldsymbol{C}_f$	branch-from incidence matrix
$\boldsymbol{C}_g$	generator incidence matrix
$\boldsymbol{C}_t$	branch-to incidence matrix
$\boldsymbol{p}_\ell^{\Delta\theta}$, $\boldsymbol{p}_\ell^{\Delta v}$	active power loss vectors generated by voltage angle differences and magnitudes
$\boldsymbol{p}_f$	active power flow at from ends
$\boldsymbol{p}_g$	decision vector active generator power
$\boldsymbol{q}_\ell^{\Delta\theta}$, $\boldsymbol{q}_\ell^{\Delta v}$	reactive power loss vectors generated by voltage angle differences and magnitudes
$\boldsymbol{q}_f$	reactive power flow at from ends
$\boldsymbol{q}_g$	decision vector reactive generator power
$\boldsymbol{s}$	apparent power line limit
$\boldsymbol{x}$, $\boldsymbol{x}'$, $\boldsymbol{x}''$	decision vectors LOLIN-OPF, LIN-OPF, MIP-OPF
$\boldsymbol{x}_{pf}$, $\boldsymbol{x}_s$	solution vectors from power flow and optimization
$\boldsymbol{Y}'_b$	adjusted nodal admittance matrix
$\boldsymbol{Y}'_f$, $\boldsymbol{Y}'_t$	adjusted branch-from and -to admittance matrices
$\boldsymbol{Y}_b$	nodal admittance matrix
$\boldsymbol{Y}_f$, $\boldsymbol{Y}_t$	branch-from and -to admittance matrices
$b \in \boldsymbol{b}$	per unit line susceptance vector
b_c	charge susceptance
f_p, f_q	linear or quadratic cost function on active and reactive generator power
f_z	objective value of problem z
$g \in \boldsymbol{g}$	per unit line conductance vector
k_1, k_2	linear loss gradient parameters
M	big M constant
n_b, n_g, n_l	number of buses, generators, and lines
$p_k \in \boldsymbol{p}$, $\boldsymbol{p}_d$	nodal active power and load
p_ℓ	active power loss
$q_k \in \boldsymbol{q}$, $\boldsymbol{q}_d$	nodal reactive power and load
q_ℓ	reactive power loss
$\boldsymbol{r}$	per unit tap ratio
$v_k \in \boldsymbol{v}$	decision vector voltage magnitudes
y	complex series admittance
y_{sh}	shunt admittance
y'^i_{ff}, y'^i_{tt}	adjusted admittance parameters
y^i_{ff}, y^i_{ft}, y^i_{tf}, y^i_{tt}	admittance parameters to describe standard π branch model

In sum, there is still a clear need of linear OPF approximations that work in the full decision variable space and capture power losses. Hence, the objective of this paper is to find a linear and tractable approximation of the OPF problem in the full decision variable space of active/reactive power and voltage magnitudes/angles for general grid topologies.

1.2. Related work

Finding reasonable linear power flow approximations for OPF problems is not a new research field. The first approaches included linearizing the power flow equations and passing this information to a Linear Programming (LP) solver. However, since this approximation does not hold for the entire operating range, the LP problem needs to be solved multiple times in an iterative way. Several papers [15–17] have used this solution approach, where they build the Jacobian of the power flow equations at a given operating point. The work featured in [18–21] derives a linear approximation of the AC power flow equations, but does not show how these approximations can be incorporated into an OPF problem. The well-known DC-OPF is extended by a piecewise affine (PWA) loss model in [18,22] to capture active power losses. However, these approaches only work in the active power domain. The authors of [23,24] suggested a linearized full OPF model with a power loss approximation. If the power losses are included as LP relaxations in the power balance constraints as done in [23], then the loss approximations will not be tight for negative locational prices (LMPs) on the power balance constraints, since fictitious losses would be generated that give the generation units more leeway to reduce the objective. The authors of [23] cope with this issue by penalizing the active power losses in the objective, which can distort the objective value especially if the system is subject to heavy loading conditions. In contrast, [24] solves the fictitious losses problem by introducing an MIP PWA loss formulation for active and reactive power losses that is harder to solve as an LP problem. The authors of [24] also prove that an LP relaxation of the active power losses only holds for positive LMPs on the active power balance constraints if the reactive power losses are neglected. In [25], Mhanna et al. approximate the second order cone relaxations with linear relaxations resulting in a high number of linear constraints. Castillo et al. [26] use also an iterative approach to compute the optimal generator setpoints by solving multiple optimization problems. The linear OPF method of [27] does not capture losses and only operates in the decision variable domain of voltage angles and active power.

1.3. Contribution

This paper deals with the development of novel tractable Linear/Quadratic Programming (LP/QP) based OPF methods that approximate the power flow over a broader operating range. The contributions of this paper are:

- Unlike [27] our OPF methods link the full decision variable domain with linear power flow approximations and capture the power losses by using absolute value loss approximations. The presented approaches are general to reflect any grid topology (meshed and radial) and any voltage levels (low voltage, distribution, and transmission grids). To our knowledge there is no existing work that have shown this feature.
- Instead of solving several optimization problems as proposed e.g. in [26] our methods can be solved in a single shot fashion by using off-the-shelf LP/QP solvers making them suitable for large-scale grid applications.
- In contrast to [23,25] our methods can deal with the fictitious losses problem by using the minimum number of power loss constraints and without penalizing the objective.
- We showed by simulation that our approaches produce feasible AC solutions, if approximate solutions exist. The computational complexity of our methods is much lower as compared to the nonlinear AC-OPF, while the objective value deviation is reasonable for typical test cases.

Fig. 1 shows the relationships between the sections of the paper. The remainder of this paper is organized as follows. Section 2 derives the power flow, loss and branch flow approximations. Section 3 shows how these approximations can be combined and included into LP/QP based

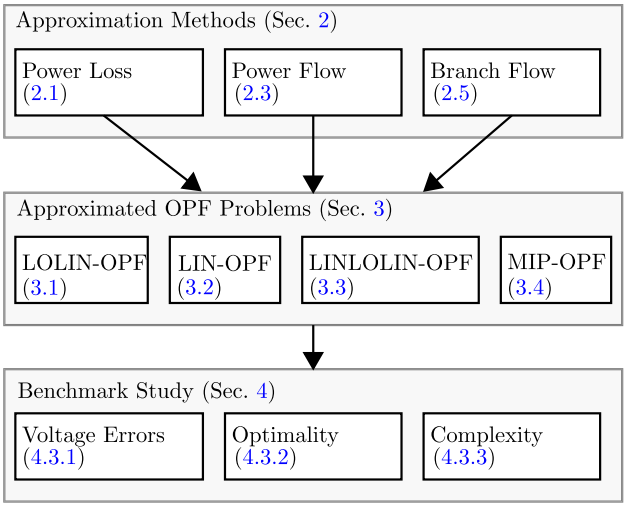

Fig. 1. Relationships between the sections of the paper.

OPF formulations. Section 4 deals with a benchmark study that analyzes the accuracy and optimality of our suggested OPF methods. Section 5 draws the conclusion.

2. Approximation methods

We first derive an absolute loss approximation based on a two-bus system example and present a linear power flow approximation. We combine these approximations and extend this result to capture tap ratios, shunt elements, and line charging. Then, we introduce nodal admittance matrices to reflect any grid topology and size and incorporate this representation into several optimal power flow problems that have different features and are compliant with an LP/QP framework.

Based on Fig. 2, the nodal active p_1, p_2 and reactive q_1, q_2 powers are given by the nonlinear AC power flow equations that are for this case

$$\begin{aligned} p_1 &= v_1^2 g - v_1 v_2 \cos(\theta_1 - \theta_2) g - v_1 v_2 \sin(\theta_1 - \theta_2) b, \\ p_2 &= v_2^2 g - v_2 v_1 \cos(\theta_2 - \theta_1) g - v_2 v_1 \sin(\theta_2 - \theta_1) b, \\ q_1 &= -v_1^2 b + v_1 v_2 \cos(\theta_1 - \theta_2) b - v_1 v_2 \sin(\theta_1 - \theta_2) g, \\ q_2 &= -v_2^2 b + v_2 v_1 \cos(\theta_2 - \theta_1) b - v_2 v_1 \sin(\theta_2 - \theta_1) g, \end{aligned} \tag{1}$$

where v_1, v_2 are the per unit nodal voltage magnitudes, θ_1, θ_2 are the voltage angles, g is the per unit line conductance and b the per unit line susceptance.

2.1. Absolute loss approximation

Existing work focuses on power loss models that capture active power losses [28,22,24]. While [22,24] use PWA models representing linear constraints in voltage angles, Martin et al. showed the importance on incorporating voltage magnitudes to improve the approximation quality. However, these works consider transmission networks and need a higher number of linear constraints, which increases the problem complexity. In contrast, our power loss approximation captures active and reactive power losses and reduces the amount of constraints at the cost of optimality. Here, an absolute value formulation, which is derived in this section, constitutes the minimum size of constraints.

The incurred active p_ℓ and reactive q_ℓ power losses for the two-bus system can be calculated by

$$p_\ell = p_1 + p_2 = (v_1^2 + v_2^2) g - 2 v_1 v_2 \cos(\theta_1 - \theta_2) g, \tag{2}$$

$$q_\ell = q_1 + q_2 = -(v_1^2 + v_2^2) b + 2 v_1 v_2 \cos(\theta_1 - \theta_2) b. \tag{3}$$

Let $v_1, v_2 = 1$ then we can find an absolute power loss approximation as a function of the voltage angle difference for active and reactive power as follows

$$p_\ell = 2(1 - \cos(\theta_1 - \theta_2)) g \approx |\theta_1 - \theta_2| 2 k_1 g, \tag{4}$$

$$q_\ell = -2(1 - \cos(\theta_1 - \theta_2)) b \approx -|\theta_1 - \theta_2| 2 k_1 b, \tag{5}$$

where k_1 is a constant that represents the gradient of the absolute function associated with the voltage angle difference. Here, we approximate $(1 - \cos(\theta_1 - \theta_2))$ with $k_1 |\theta_1 - \theta_2|$. If we let $\theta_1 - \theta_2 = 0$ then we obtain approximations in terms of absolute values that are functions of the voltage magnitude difference:

$$p_\ell = (v_1 - v_2)^2 g \approx |v_1 - v_2| 2 k_2 g, \tag{6}$$

$$q_\ell = -(v_1 - v_2)^2 b \approx -|v_1 - v_2| 2 k_2 b, \tag{7}$$

where k_2 is a constant to approximate the losses associated with the voltage magnitude difference. Here, we approximate $(v_1 - v_2)^2$ with $|v_1 - v_2| 2 k_2$.

By superposing the approximations (4) and (6) and superposing the approximations (5) and (7), we approximate the active p_ℓ^{approx} and reactive power losses q_ℓ^{approx} as follows:

$$p_\ell^{\text{approx}} = \underbrace{|\theta_1 - \theta_2| 2 k_1 g}_{2 p_\ell^{\Delta\theta}} + \underbrace{|v_1 - v_2| 2 k_2 g}_{2 p_\ell^{\Delta v}}, \tag{8}$$

$$q_\ell^{\text{approx}} = \underbrace{-|\theta_1 - \theta_2| 2 k_1 b}_{2 q_\ell^{\Delta\theta}} - \underbrace{|v_1 - v_2| 2 k_2 b}_{2 q_\ell^{\Delta v}}, \tag{9}$$

that are convex reformulations of the exact power losses (2) and (3).

2.2. Selection of k_1, k_2

We have two degrees of freedom to approximate the power losses with the constants k_1, k_2. To parametrize those parameters we define the design parameters $\Delta\theta_d = \theta_1 - \theta_2$, $\Delta v_d = v_1 - v_2$. They specify a usual voltage magnitude and angle difference between two nodes that are connected by a line. If we solve the Eqs. (4), (5) for k_1 and (6), (7) for k_2, we obtain the following parametrizations for k_1, k_2

$$k_1 = \frac{1 - \cos\Delta\theta_d}{|\Delta\theta_d|} \approx \frac{|\Delta\theta_d|}{2}, \tag{10}$$

$$k_2 = \frac{|\Delta v_d|}{2}. \tag{11}$$

The quality of the loss approximation depends strongly on the loading of the system and the selection of k_1, k_2. The errors can be reduced by evaluating the approximations around the operating points. Instead of optimizing k_1, k_2 for each specific load case, we choose typical static values for $\Delta\theta_d = 0.05$ rad, $\Delta v_d = 0.02$ p.u. by calculating the mean value of angular and magnitude differences obtained from typical load cases. This is different as proposed in [23], where a base case is needed to calculate grid specific loss factors. With this approach we weight the losses with respect to the susceptances and conductances. In this way it is possible to consider general grid topologies ranging from low voltage grids usually having a high R/X ratio to transmission grids possessing a high X/R ratio. Fig. 3a and b show the exact and the approximated

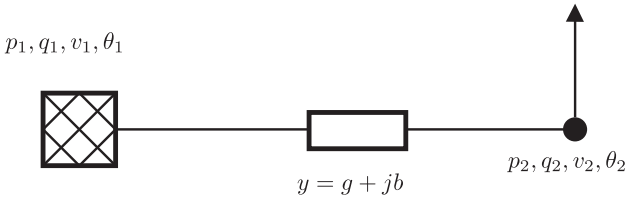

Fig. 2. Two-bus system to illustrate and derive the linear power flow and absolute loss approximations.

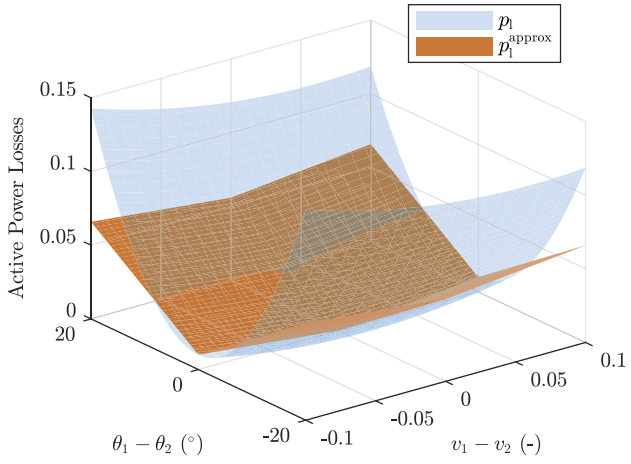

(a) Active power losses

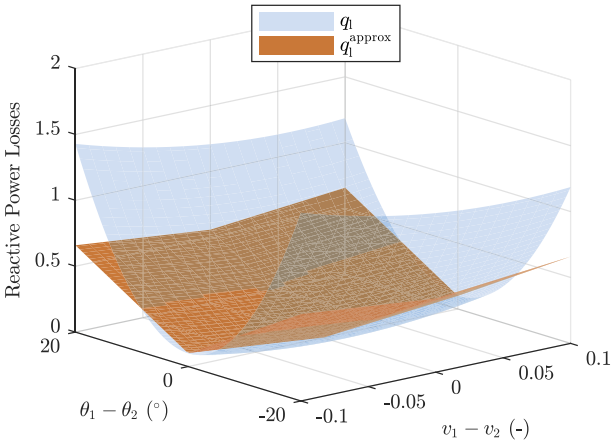

(b) Reactive power losses

Fig. 3. Power loss comparison for the parameters $b = -10$ and $g = 1$. The blue surface indicates the exact losses, while the red surfaces are the absolute power loss approximations. (For interpretation of the references to color in this figure legend, the reader is referred to the web version of this article.)

power losses for the two-bus transmission system (Fig. 2) with the per unit susceptance $b = -10$ and the per unit conductance $g = 1$. Note that this formulation is an approximation and not a relaxation, since there are loss regions that are underestimated above the values $\Delta\theta_d$ and Δv_d. This means that these errors translate to an underestimation of voltage angles and magnitudes. Hence, there is no guarantee that the approximated OPF solutions will lie inside the feasible original solution space.

2.3. Linear power flow approximation

We linearize the nonlinear power flow Eqs. (1) by using the following approximations[1]:

$$\cos(\theta_i - \theta_j) \approx 1, \tag{12}$$

$$v_i^2 - v_i v_j \approx v_i - v_j, \tag{13}$$

$$v_i v_j \sin(\theta_i - \theta_j) \approx (\theta_i - \theta_j), \tag{14}$$

to obtain

$$\begin{aligned} p_1 &\approx (v_1 - v_2)g - (\theta_1 - \theta_2)b + p_\ell^{\Delta\theta} + p_\ell^{\Delta v}, \\ p_2 &\approx (v_2 - v_1)g - (\theta_2 - \theta_1)b + p_\ell^{\Delta\theta} + p_\ell^{\Delta v}, \\ q_1 &\approx -(v_1 - v_2)b - (\theta_1 - \theta_2)g + q_\ell^{\Delta\theta} + q_\ell^{\Delta v}, \\ q_2 &\approx -(v_2 - v_1)b - (\theta_2 - \theta_1)g + q_\ell^{\Delta\theta} + q_\ell^{\Delta v}, \end{aligned} \tag{15}$$

in which we also add the convex reformulations of the power losses $p_\ell^{\Delta v}$, $q_\ell^{\Delta v}$, $p_\ell^{\Delta\theta}$, $q_\ell^{\Delta\theta}$ derived from the previous Section 2.1. As a result, the power flow approximations (15) are convex, which can also be graphically verified in Fig. 4a and b. However, if these approximations are incorporated as power balance constraints in the OPF problem, then the nested absolute value functions (8) and (9) make the constraints non-convex. For this reason, we relax the problem to a convex one by incorporating their epigraphs as linear constraints.

The terms in b for the nodal active powers p_1, p_2 correspond to the DC power flow approximation. All terms in b correspond to the fast decoupled load flow expressions evaluated at the first iteration [29]. However, the only difference is that we still have remaining expressions in g that are crucial to capture power flows in distribution grids. The power flow approximations (15) follow the same structure as presented in [20], but are extended with the power losses. In contrast to [23], we do not use squared expressions for the voltage magnitudes. Instead of using a power flow representation in rectangular coordinates as proposed in [30], we approximate the power flow in polar coordinates.

2.4. Extension for line charging, transformer tap ratios and shunts

The aforementioned two-bus system example considers only a series admittance y. In this section, we aim to extend our approach to incorporate line charging, transformer tap ratios and shunt elements. To capture these features, we use the standard π branch model. The nodal admittance matrix $\boldsymbol{Y}_b$ for the two-bus system is then e.g.

$$\boldsymbol{Y}_b = \begin{bmatrix} y_{ff}^i & y_{ft}^i \\ y_{tf}^i & y_{tt}^i \end{bmatrix} = \begin{bmatrix} \left(y + j\frac{b_c}{2}\right)\frac{1}{\tau^2} & -y\frac{1}{\tau e^{-\theta_s}} \\ -y\frac{1}{\tau e^{\theta_s}} & \left(y + j\frac{b_c}{2}\right) \end{bmatrix}, \tag{16}$$

where $y = g + jb$ is the complex series admittance, τ is the per unit tap ratio, θ_s is the transformer shift angle, b_c is the per unit capacitive reactance of the line. We also define the matrix $\boldsymbol{Y}'_b$, in which we only consider the series admittance with the complex tap ratios as follows

$$\boldsymbol{Y}'_b = \begin{bmatrix} y_{ff}'^i & y_{ft}^i \\ y_{tf}^i & y_{tt}'^i \end{bmatrix} = \begin{bmatrix} y\frac{1}{\tau e^{-\theta_s}} & -y\frac{1}{\tau e^{-\theta_s}} \\ -y\frac{1}{\tau e^{\theta_s}} & y\frac{1}{\tau e^{\theta_s}} \end{bmatrix}. \tag{17}$$

This matrix is needed for the power flow approximation to correctly represent the power flow contribution on the voltage angles.

In the same notation of [31] we next generalize our approach to account for any grid topology. First, we define a grid that consists of n_b buses, n_g generators, and n_l lines. Any topology can be specified by constructing the node-branch incidence matrix $\boldsymbol{C}_{br} \in \mathbb{Z}^{n_l \times n_b}$, from which we can derive the node-branch-from and node-branch-to incidence matrices $\boldsymbol{C}_f$, $\boldsymbol{C}_t \in \mathbb{Z}^{n_l \times n_b}$. We introduce the generator active and reactive power injections $\boldsymbol{p}_g$, $\boldsymbol{q}_g \in \mathbb{R}^{n_g \times 1}$. The generator to bus mapping is specified with the matrix $\boldsymbol{C}_g \in \mathbb{Z}^{n_g \times n_b}$.

The branch-from and -to admittance matrices $\boldsymbol{Y}_f$, $\boldsymbol{Y}_t \in \mathbb{C}^{n_l \times n_b}$ are calculated as

$$\boldsymbol{Y}_f = \text{diag}\left\{y_{ff}^1, \ldots, y_{ff}^{n_l}\right\}\boldsymbol{C}_f + \text{diag}\left\{y_{ft}^1, \ldots, y_{ft}^{n_l}\right\}\boldsymbol{C}_t, \tag{18}$$

$$\boldsymbol{Y}_t = \text{diag}\left\{y_{tf}^1, \ldots, y_{tf}^{n_l}\right\}\boldsymbol{C}_f + \text{diag}\left\{y_{tt}^1, \ldots, y_{tt}^{n_l}\right\}\boldsymbol{C}_t. \tag{19}$$

In the same straightforward way the adjusted versions of the branch admittance matrices $\boldsymbol{Y}'_f$, $\boldsymbol{Y}'_t \in \mathbb{C}^{n_l \times n_b}$ are

[1] Note that the DC power flow uses the same approximation (14) and the fast-decoupled power flow [29] makes use of the approximation (12).

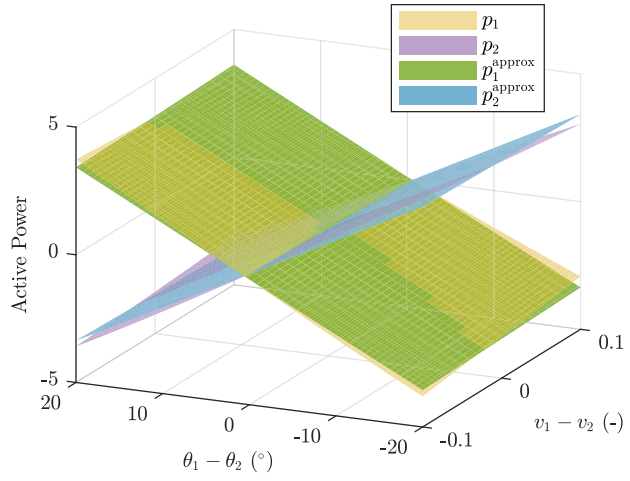

(a) Active power

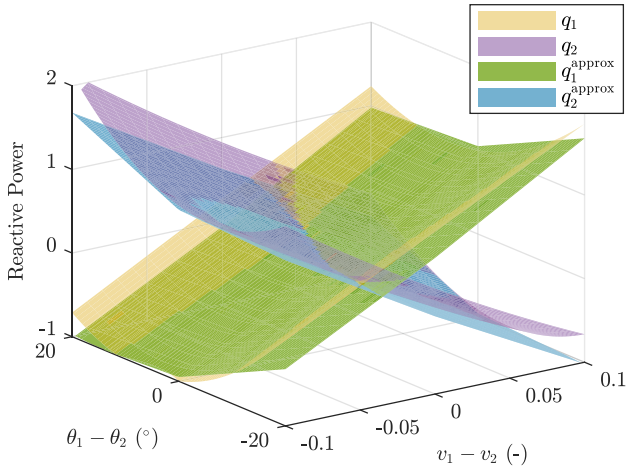

(b) Reactive power

Fig. 4. Power flow comparison. p_1, p_2 represent the nonlinear power flow Eqs. (1) and p_1^{approx}, p_2^{approx} are the convex power flow approximations (15).

$$\boldsymbol{Y}'_{\mathrm{f}} = \mathrm{diag}\left\{y'^{1}_{ff}, \ldots, y'^{n_{\mathrm{l}}}_{ff}\right\}\boldsymbol{C}_{\mathrm{f}} + \mathrm{diag}\left\{y^{1}_{ft}, \ldots, y^{n_{\mathrm{l}}}_{ft}\right\}\boldsymbol{C}_{\mathrm{t}}, \tag{20}$$

$$\boldsymbol{Y}'_{\mathrm{t}} = \mathrm{diag}\left\{y^{1}_{tf}, \ldots, y^{n_{\mathrm{l}}}_{tf}\right\}\boldsymbol{C}_{\mathrm{f}} + \mathrm{diag}\left\{y'^{1}_{tt}, \ldots, y'^{n_{\mathrm{l}}}_{tt}\right\}\boldsymbol{C}_{\mathrm{t}}, \tag{21}$$

in which we neglect the shunt admittances and line capacitances.

The nodal admittance matrix $\boldsymbol{Y}_{\mathrm{b}} \in \mathbb{C}^{n_{\mathrm{b}} \times n_{\mathrm{b}}}$, and its adjusted version $\boldsymbol{Y}'_{\mathrm{b}} \in \mathbb{C}^{n_{\mathrm{b}} \times n_{\mathrm{b}}}$ are determined by

$$\boldsymbol{Y}_{\mathrm{b}} = \boldsymbol{C}_{\mathrm{f}}^{T}\boldsymbol{Y}_{\mathrm{f}} + \boldsymbol{C}_{\mathrm{t}}^{T}\boldsymbol{Y}_{\mathrm{t}} + \mathrm{diag}\{y^{1}_{\mathrm{sh}}, \ldots, y^{n_b}_{\mathrm{sh}}\}, \tag{22}$$

$$\boldsymbol{Y}'_{\mathrm{b}} = \boldsymbol{C}_{\mathrm{f}}^{T}\boldsymbol{Y}'_{\mathrm{f}} + \boldsymbol{C}_{\mathrm{t}}^{T}\boldsymbol{Y}'_{\mathrm{t}}, \tag{23}$$

where y^{i}_{sh} are the per unit shunt admittances.

We extend the decision variables θ, $\boldsymbol{v} \in \mathbb{R}^{n_{\mathrm{b}} \times 1}$, $\boldsymbol{p}_{\ell}^{\Delta\theta}$, $\boldsymbol{p}_{\ell}^{\Delta v}$, $\boldsymbol{q}_{\ell}^{\Delta\theta}$, $\boldsymbol{q}_{\ell}^{\Delta v} \in \mathbb{R}^{n_{\mathrm{l}} \times 1}$ to reflect any grid topology. The nodal active and reactive power injections $\boldsymbol{p}$, $\boldsymbol{q} \in \mathbb{R}^{n_{\mathrm{b}} \times 1}$ are split into

$$\boldsymbol{p} = \boldsymbol{C}_{\mathrm{g}}\boldsymbol{p}_{\mathrm{g}} - \boldsymbol{p}_{\mathrm{d}}, \tag{24}$$

$$\boldsymbol{q} = \boldsymbol{C}_{\mathrm{g}}\boldsymbol{q}_{\mathrm{g}} - \boldsymbol{q}_{\mathrm{d}}, \tag{25}$$

where $\boldsymbol{p}_{\mathrm{d}}$, $\boldsymbol{q}_{\mathrm{d}} \in \mathbb{R}^{n_{\mathrm{b}} \times 1}$ are the active and reactive load vectors.

Under these definitions, we can find a more general matrix representation for the active power flow approximation as

$$\begin{bmatrix} -\Im\{\boldsymbol{Y}'_{\mathrm{b}}\} & \Re\{\boldsymbol{Y}_{\mathrm{b}}\} & -\boldsymbol{C}_{\mathrm{g}} & |\boldsymbol{C}_{\mathrm{br}}|^{T} & |\boldsymbol{C}_{\mathrm{br}}|^{T} \end{bmatrix} \begin{bmatrix} \theta \\ \boldsymbol{v} \\ \boldsymbol{p}_{\mathrm{g}} \\ \boldsymbol{p}_{\ell}^{\Delta\theta} \\ \boldsymbol{p}_{\ell}^{\Delta v} \end{bmatrix} = -\boldsymbol{p}_{\mathrm{d}}, \tag{26}$$

and for the reactive power flow as

$$\begin{bmatrix} -\Re\{\boldsymbol{Y}'_{\mathrm{b}}\} & -\Im\{\boldsymbol{Y}_{\mathrm{b}}\} & -\boldsymbol{C}_{\mathrm{g}} & |\boldsymbol{C}_{\mathrm{br}}|^{T} & |\boldsymbol{C}_{\mathrm{br}}|^{T} \end{bmatrix} \begin{bmatrix} \theta \\ \boldsymbol{v} \\ \boldsymbol{q}_{\mathrm{g}} \\ \boldsymbol{q}_{\ell}^{\Delta\theta} \\ \boldsymbol{q}_{\ell}^{\Delta v} \end{bmatrix} = -\boldsymbol{q}_{\mathrm{d}}, \tag{27}$$

where $\Re$, $\Im$ denote the real and imaginary part of a complex number. Note that (26) and (27) capture the approximated power flow Eqs. (15) for the two-bus system if (16) and (17) are inserted.

2.5. Branch flow approximation

To obtain tractable OPF problems, we linearly approximate the active and reactive power line flows at the from ends $\boldsymbol{p}_{\mathrm{f}}$, $\boldsymbol{q}_{\mathrm{f}} \in \mathbb{R}^{n_{\mathrm{l}} \times 1}$ as

$$\boldsymbol{p}_{\mathrm{f}} = -\Im\{\boldsymbol{Y}'_{\mathrm{f}}\}\theta + \Re\{\boldsymbol{Y}_{\mathrm{f}}\}\boldsymbol{v}, \tag{28}$$

$$\boldsymbol{q}_{\mathrm{f}} = -\Re\{\boldsymbol{Y}'_{\mathrm{f}}\}\theta - \Im\{\boldsymbol{Y}_{\mathrm{f}}\}\boldsymbol{v}. \tag{29}$$

Note that the power line losses are neglected by using this formulation.

3. Approximated tractable optimal power flow problems

In this section we derive the formulations of the approximated OPF problems. Table 1 summarizes the suggested methods listed by their names and their capabilities indicated by the label ('x'). We developed four OPF methods, in which three of them are defined as LP/QP problems and one is formulated as an MILP/MIQP problem. The first LP/QP based method LOLIN-OPF includes the active power losses p_{ℓ} as epigraphs to the active power balance constraints, discards the reactive power losses q_{ℓ} and is only valid for non-negative LMPs on the active power balance constraints p. The second method LIN-OPF discards active and reactive power losses. The third method LINLOLIN-OPF is a combination of the first two aforementioned methods and considers active power losses. The fourth method MIP-OPF includes reactive and active power losses.

3.1. Lossy LP/QP based Optimal Power Flow (LOLIN-OPF) problem

With the introduced power flow approximations we can now formulate the OPF problem within a standard LP/QP framework. We specify the decision vector $\boldsymbol{x} = [\theta\ \boldsymbol{v}\ \boldsymbol{p}_{\mathrm{g}}\ \boldsymbol{q}_{\mathrm{g}}\ \boldsymbol{p}_{\ell}^{\Delta\theta}\ \boldsymbol{p}_{\ell}^{\Delta v}\ \boldsymbol{q}_{\ell}^{\Delta\theta}\ \boldsymbol{q}_{\ell}^{\Delta v}]^{T}$. The objective of the OPF problem is to find the optimal active and reactive generator powers that minimize either a linear or quadratic cost objective. The approximated lossy LP/QP based Optimal Power Flow (LOLIN-OPF) problem is

Table 1
Comparison of suggested methods.

Method	Problem	Modeling of Power Losses on		Compatible with Negative LMPs on	
		p_{ℓ}	q_{ℓ}	p	q
LOLIN-OPF	LP/QP	x	–	–	x
LIN-OPF	LP/QP	–	–	x	x
LINLOLIN-OPF	LP/QP	x	–	x	x
MIP-OPF	MILP/MIQP	x	x	x	x

$$
\begin{aligned}
\text{LOLIN-OPF:}\quad & \min_{\boldsymbol{x}} \quad f_p(\boldsymbol{p}_\mathrm{g}) + f_q(\boldsymbol{q}_\mathrm{g}) \\
& \text{s.t.} \quad (26),\ (27) \\
& (a) \quad k_\mathrm{l}\,\mathrm{diag}\{\boldsymbol{g}\}\boldsymbol{C}_\mathrm{br}\theta - \boldsymbol{p}_\ell^{\Delta\theta} \leqslant \boldsymbol{0} \\
& (b) \quad -k_\mathrm{l}\,\mathrm{diag}\{\boldsymbol{g}\}\boldsymbol{C}_\mathrm{br}\theta - \boldsymbol{p}_\ell^{\Delta\theta} \leqslant \boldsymbol{0} \\
& (c) \quad k_2\,\mathrm{diag}\{\boldsymbol{g}\}\boldsymbol{C}_\mathrm{br}\boldsymbol{v} - \boldsymbol{p}_\ell^{\Delta v} \leqslant \boldsymbol{0} \\
& (d) \quad -k_2\,\mathrm{diag}\{\boldsymbol{g}\}\boldsymbol{C}_\mathrm{br}\boldsymbol{v} - \boldsymbol{p}_\ell^{\Delta v} \leqslant \boldsymbol{0} \\
& (e) \quad k_\mathrm{l}\,\mathrm{diag}\{\boldsymbol{b}\}\boldsymbol{C}_\mathrm{br}\theta - \boldsymbol{q}_\ell^{\Delta\theta} \leqslant \boldsymbol{0} \\
& (f) \quad -k_\mathrm{l}\,\mathrm{diag}\{\boldsymbol{b}\}\boldsymbol{C}_\mathrm{br}\theta - \boldsymbol{q}_\ell^{\Delta\theta} \leqslant \boldsymbol{0} \\
& (g) \quad k_2\,\mathrm{diag}\{\boldsymbol{b}\}\boldsymbol{C}_\mathrm{br}\boldsymbol{v} - \boldsymbol{q}_\ell^{\Delta v} \leqslant \boldsymbol{0} \\
& (h) \quad -k_2\,\mathrm{diag}\{\boldsymbol{b}\}\boldsymbol{C}_\mathrm{br}\boldsymbol{v} - \boldsymbol{q}_\ell^{\Delta v} \leqslant \boldsymbol{0} \\
& (i) \quad -\boldsymbol{s} \leqslant \boldsymbol{p}_\mathrm{f} + \boldsymbol{A}_q\boldsymbol{q}_\mathrm{f} \leqslant \boldsymbol{s} \\
& (j) \quad -\boldsymbol{s} \leqslant \boldsymbol{p}_\mathrm{f} - \boldsymbol{A}_q\boldsymbol{q}_\mathrm{f} \leqslant \boldsymbol{s} \\
& (k) \quad -\boldsymbol{s} \leqslant \boldsymbol{A}_q\boldsymbol{p}_\mathrm{f} + \boldsymbol{q}_\mathrm{f} \leqslant \boldsymbol{s} \\
& (l) \quad -\boldsymbol{s} \leqslant \boldsymbol{A}_q\boldsymbol{p}_\mathrm{f} - \boldsymbol{q}_\mathrm{f} \leqslant \boldsymbol{s},
\end{aligned} \tag{30}
$$

where f_p, f_q are either linear or quadratic generator cost functions. The constraints (26), (27) specify the nodal active and reactive power balance equations. The inequalities (30)a–h represent the epigraphs of the approximated absolute power loss functions derived in (8) and (9) and can be regarded as LP relaxations. It is noteworthy that the power loss vectors only lie on these hyperplanes if the Lagrange multipliers on the active and reactive power balance constraints (26) and (27) are non-negative. In other words the constraints (30)a–h need to be binding to achieve a physical meaningful solution. Negative multipliers (also called LMPs) would lead to fictitious losses allowing to consume more active or reactive power to lower the objective value. Negative LMPs could occur in highly congested systems or for negative cost functions. Since we often have the case that generator cost functions are specified in the active power domain only, it is common to have negative LMPs on the reactive power balance constraints, which means that we can only find tractable approximations by neglecting reactive power losses. In addition, it was shown in [24] that the active loss LP relaxations only hold for non-negative LMPs on the active power balance, if the reactive power losses are neglected. Due to these reasons, we remove the reactive power loss variables $\boldsymbol{q}_\ell^{\Delta v}$, $\boldsymbol{q}_\ell^{\Delta\theta}$ from the problem and discard the constraints (30)e–h at the cost of accuracy. To deal with negative LMPs on the active power balance constraints, we introduce a consecutive method that is described in Section 3.3. To generally include active and reactive power losses, we will formulate an MIP problem that will be discussed in Section 3.4. The constraints (30)i–l define convex polygons to approximate the circular PQ capability area. The vector $\boldsymbol{s} \in \mathbb{R}^{n_\mathrm{l}\times 1}$ specifies the apparent power line limits and $\boldsymbol{A}_q = \mathrm{diag}\{\boldsymbol{a}_q \in \mathbb{R}^{n_\mathrm{l}\times 1}\}$ represents the derivatives of the lines that form a convex polygon as shown in Fig. 5. Here, we consider 8 convex segments to approximate the circular PQ area.

3.2. Lossless LP/QP based Optimal Power Flow (LIN-OPF) problem

If the LOLIN-OPF problem returns negative LMPs on the active power balance and we would like to avoid solving an MIP problem, we can define a lossless version of the OPF problem at the cost of accuracy. We eliminate the power loss vectors from (26) and (27), so that the decision vector is $\boldsymbol{x}' = [\theta\ \boldsymbol{v}\ \boldsymbol{p}_\mathrm{g}\ \boldsymbol{q}_\mathrm{g}]^T$. Then, the lossless LP/QP based Optimal Power Flow (LIN-OPF) problem is:

$$
\begin{aligned}
\text{LIN-OPF:}\quad & \min_{\boldsymbol{x}'} \quad f_p(\boldsymbol{p}_\mathrm{g}) + f_q(\boldsymbol{q}_\mathrm{g}) \\
& \text{s.t.} \quad (30\text{i–l}) \\
& (a) \quad -\Im\{\boldsymbol{Y}'_\mathrm{b}\}\theta + \Re\{\boldsymbol{Y}_\mathrm{b}\}\boldsymbol{v} - \boldsymbol{C}_\mathrm{g}\boldsymbol{p}_\mathrm{g} = -\boldsymbol{p}_\mathrm{d} \\
& (b) \quad -\Re\{\boldsymbol{Y}'_\mathrm{b}\}\theta - \Im\{\boldsymbol{Y}_\mathrm{b}\}\boldsymbol{v} - \boldsymbol{C}_\mathrm{g}\boldsymbol{q}_\mathrm{g} = -\boldsymbol{q}_\mathrm{d}.
\end{aligned} \tag{31}
$$

3.3. Consecutive lossy LP/QP based Optimal Power Flow (LINLOLIN-OPF) problem

By solving the previous LIN-OPF method and running a second optimization problem it is possible to consider power losses for negative LMPs. For the second problem, we modify the LOLIN-OPF problem (30) by fixing the power loss constraints with respect to the LIN-OPF solution. In particular, we equalize the power loss constraints (30)a–d that are active in the directions of the voltage magnitude and angle differences obtained from the LIN-OPF solution and discard the remaining constraints being not active associated with the LIN-OPF solution.

3.4. Mixed Integer LP/QP based Optimal Power Flow (MIP-OPF) problem

As discussed in Section 3.1 the optimal solution might not be binding with respect to the power loss constraints. An alternative but computationally more expensive formulation can be obtained by expressing the power loss constraints through an MIP approach. For this, we restructure the decision vector to $\boldsymbol{x}'' = [\theta\ \boldsymbol{v}\ \boldsymbol{p}_\mathrm{g}\ \boldsymbol{q}_\mathrm{g}\ \Delta\theta\ \Delta\boldsymbol{v}\ \boldsymbol{b}^\theta\ \boldsymbol{b}^v]^T$. The power loss vectors are now replaced by $\Delta\theta$, $\Delta\boldsymbol{v} \in \mathbb{R}^{n_\mathrm{l}\times 1}$ specifying the absolute values of $|\theta_i - \theta_j|$ and $|v_i - v_j|$ in (8) and (9). We introduce the binary variables $\boldsymbol{b}^\theta$, $\boldsymbol{b}^v \in \mathbb{Z}^{n_\mathrm{l}\times 1}$ that are associated with $\Delta\theta$, $\Delta\boldsymbol{v}$. The approximated active and reactive power balance can be adjusted to comply with the new introduced decision vectors $\Delta\theta$, $\Delta\boldsymbol{v}$ as

$$
\begin{bmatrix}
-\Im\{\boldsymbol{Y}'_\mathrm{b}\} & \Re\{\boldsymbol{Y}_\mathrm{b}\} & -\boldsymbol{C}_\mathrm{g} & \boldsymbol{0} \\
-\Re\{\boldsymbol{Y}'_\mathrm{b}\} & -\Im\{\boldsymbol{Y}_\mathrm{b}\} & \boldsymbol{0} & -\boldsymbol{C}_\mathrm{g} \\
k_\mathrm{l}\,\mathrm{diag}\{\boldsymbol{g}\}|\boldsymbol{C}_\mathrm{br}|^T & k_2\,\mathrm{diag}\{\boldsymbol{g}\}|\boldsymbol{C}_\mathrm{br}|^T & \boldsymbol{0} & \boldsymbol{0} \\
k_\mathrm{l}\,\mathrm{diag}\{\boldsymbol{b}\}|\boldsymbol{C}_\mathrm{br}|^T & k_2\,\mathrm{diag}\{\boldsymbol{b}\}|\boldsymbol{C}_\mathrm{br}|^T & \boldsymbol{0} & \boldsymbol{0}
\end{bmatrix}
\begin{bmatrix}
\theta \\ \boldsymbol{v}_\mathrm{m} \\ \boldsymbol{p}_\mathrm{g} \\ \boldsymbol{q}_\mathrm{g} \\ \Delta\theta \\ \Delta\boldsymbol{v}
\end{bmatrix}
=
\begin{bmatrix}
-\boldsymbol{p}_\mathrm{d} \\ -\boldsymbol{q}_\mathrm{d}
\end{bmatrix}.
\tag{32}
$$

Then, the Mixed Integer LP/QP based Optimal Power Flow (MIP-OPF) problem is

$$
\begin{aligned}
\text{MIP-OPF:}\quad & \min_{\boldsymbol{x}''} \quad f_p(\boldsymbol{p}_\mathrm{g}) + f_q(\boldsymbol{q}_\mathrm{g}) \\
& \text{s.t.} \quad (32),\ (30\text{i–l}) \\
& (a) \quad -M(\boldsymbol{1} - \boldsymbol{b}^\theta) \leqslant -\boldsymbol{C}_\mathrm{br}\theta \leqslant M\boldsymbol{b}^\theta \\
& (b) \quad \boldsymbol{0} \leqslant -\boldsymbol{C}_\mathrm{br}\theta + \Delta\theta \leqslant 2M\boldsymbol{b}^\theta \\
& (c) \quad \boldsymbol{0} \leqslant \boldsymbol{C}_\mathrm{br}\theta + \Delta\theta \leqslant 2M(\boldsymbol{1} - \boldsymbol{b}^\theta) \\
& (d) \quad -M(\boldsymbol{1} - \boldsymbol{b}^v) \leqslant -\boldsymbol{C}_\mathrm{br}\boldsymbol{v} \leqslant M\boldsymbol{b}^v \\
& (e) \quad \boldsymbol{0} \leqslant -\boldsymbol{C}_\mathrm{br}\boldsymbol{v} + \Delta\boldsymbol{v} \leqslant 2M\boldsymbol{b}^v \\
& (f) \quad \boldsymbol{0} \leqslant \boldsymbol{C}_\mathrm{br}\boldsymbol{v} + \Delta\boldsymbol{v} \leqslant 2M(\boldsymbol{1} - \boldsymbol{b}^v),
\end{aligned} \tag{33}
$$

where the constraints (33)a–f specify a big M formulation of the absolute value functions in (8) and (9). The variable M has a considerable influence on the feasibility of the problem. It needs to be chosen

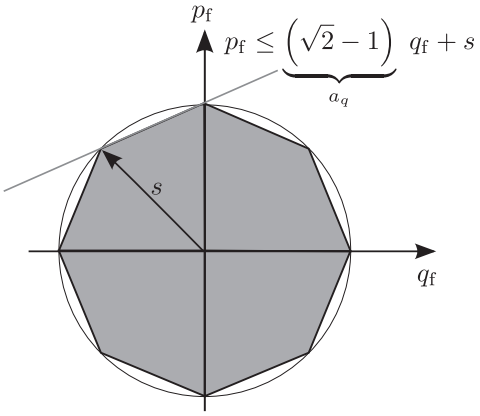

Fig. 5. Illustrative example for the convex line flow approximation for one power line. The gray line with the corresponding inequality specifies one segment of the circular PQ area.

Table 2
OPF results for PGlib [33] and MATPOWER [31] testcases including the bundled PEGASE [38] test cases.

#	Testcase	Method	Problem	Objective	ϵ_O	Magnitude Error (p.u.)			Angle Error (°)			Runtime
				($/h)	(%)	ϵ_v	$\epsilon_{\Delta v}$	max$\lvert\epsilon_{\Delta v}\rvert$	ϵ_θ	$\epsilon_{\Delta\theta}$	max$\lvert\epsilon_{\Delta\theta}\rvert$	(sec)
					MATPOWER [31] test cases							
1	case118	AC-OPF	NLP	1.297e+05	–	–	–	–	–	–	–	8.0e−01
		DC-OPF	QP	1.259e+05	2.86	n.p.	n.p.	n.p.	n.p.	n.p.	n.p.	2.7e−01
		LIN-OPF	QP	1.259e+05	2.86	0.002	0.002	0.009	1.89	0.35	1.48	2.0e−01
		LOLIN-OPF	QP	1.296e+05	0.07	0.002	0.002	0.009	0.95	0.18	0.99	3.6e−01
		MIP-OPF	MIQP	1.296e+05	0.07	0.001	0.001	0.004	0.42	0.20	0.79	3.7e+00
		DCPLL	QCP	1.299e+05	−0.15	n.p.	n.p.	n.p.	n.p.	n.p.	n.p.	1.7e+00
		QCWR	QCP	1.293e+05	0.25	0.001	0.001	0.007	5.12	1.21	4.76	7.7e−01
2	case300	AC-OPF	NLP	7.197e+05	–	–	–	–	–	–	–	3.9e−01
		DC-OPF	QP	7.063e+05	1.87	n.p.	n.p.	n.p.	n.p.	n.p.	n.p.	1.6e−01
		LIN-OPF	QP	7.063e+05	1.86	0.024	0.012	0.069	20.00	1.12	11.13	1.6e−01
		LOLIN-OPF	QP	7.180e+05	0.24	0.021	0.011	0.070	4.33	0.35	2.05	3.1e−01
		MIP-OPF	MIQP	7.181e+05	0.22	0.008	0.006	0.058	4.11	0.33	1.83	3.3e+01
		DCPLL	QCP	7.194e+05	0.04	n.p.	n.p.	n.p.	n.p.	n.p.	n.p.	1.2e−01
		QCWR	QCP	7.187e+05	0.15	0.007	0.007	0.093	3.38	1.60	10.20	2.4e+00
3	case1354pegase	AC-OPF	NLP	7.407e+04	–	–	–	–	–	–	–	1.8e+00
		DC-OPF	LP	7.306e+04	1.36	n.p.	n.p.	n.p.	n.p.	n.p.	n.p.	1.4e−01
		LIN-OPF	LP	7.306e+04	1.36	0.025	0.009	0.073	15.07	0.76	7.72	5.8e−01
		LOLIN-OPF	LP	7.475e+04	−0.92	0.019	0.006	0.060	1.13	0.35	4.80	2.4e+00
		DCPLL	QCP	7.415e+04	−0.11	n.p.	n.p.	n.p.	n.p.	n.p.	n.p.	8.5e−01
		QCWR	QCP	7.402e+04	0.07	0.002	0.001	0.011	4.63	0.82	5.77	2.5e+01
4	case33bw	AC-OPF	NLP	7.835e+01	–	–	–	–	–	–	–	1.0e+00
		DC-OPF	LP	7.430e+01	5.17	n.p.	n.p.	n.p.	n.p.	n.p.	n.p.	2.7e−01
		LIN-OPF	LP	7.430e+01	5.17	0.004	0.001	0.005	0.03	0.02	0.11	2.2e−01
		LOLIN-OPF	LP	8.231e+01	−5.05	0.001	0.001	0.002	0.11	0.04	0.13	5.0e−01
		MIP-OPF	MILP	8.089e+01	−3.24	0.001	0.000	0.001	0.03	0.02	0.11	5.9e−01
		DCPLL	QCP	7.679e+01	2.00	n.p.	n.p.	n.p.	n.p.	n.p.	n.p.	1.8e+00
		QCWR	QCP	7.835e+01	0.00	0.000	0.000	0.001	0.12	0.09	0.39	1.2e−01
5	cigre [39]	AC-OPF	NLP	−2.700e+00	–	–	–	–	–	–	–	4.8e−01
		DC-OPF	QP	−2.957e+00	−9.52	n.p.	n.p.	n.p.	n.p.	n.p.	n.p.	2.1e−01
		LIN-OPF	QP	−3.095e+00	−14.63	0.003	0.000	0.001	0.10	0.01	0.05	1.5e−01
		LOLIN-OPF	QP	−2.713e+00	−0.47	0.001	0.000	0.001	0.03	0.01	0.03	2.0e−01
		MIP-OPF	MIQP	−2.714e+00	−0.52	0.001	0.000	0.001	0.01	0.00	0.01	4.8e−01
		DCPLL	QCP	−2.692e+00	0.30	n.p.	n.p.	n.p.	n.p.	n.p.	n.p.	1.1e−02
		QCWR	QCP	−2.700e+00	0.00	0.001	0.000	0.001	1.64	0.30	1.23	8.3e−02
					PGlib [33] test cases							
6	case2869_pegase	AC-OPF	NLP	2.605e+06	–	–	–	–	–	–	–	8.0e+00
		DC-OPF	LP	2.501e+06	4.00	n.p.	n.p.	n.p.	n.p.	n.p.	n.p.	6.4e−01
		LIN-OPF	LP	2.505e+06	3.84	0.020	0.006	0.061	35.65	0.78	12.05	3.7e+00
		LINLOLIN-OPF	LP	2.646e+06	−1.59	0.020	0.006	0.056	3.37	0.32	3.77	1.2e+01
		DCPLL	QCP	2.613e+06	−0.29	n.p.	n.p.	n.p.	n.p.	n.p.	n.p.	3.2e+00
		QCWR	QCP	2.577e+06	1.07	0.003	0.001	0.016	8.15	0.61	4.94	8.4e+01
7	case9241_pegase	AC-OPF	NLP	6.775e+06	–	–	–	–	–	–	–	1.3e+03
		DC-OPF	LP	6.541e+06	3.45	n.p.	n.p.	n.p.	n.p.	n.p.	n.p.	1.5e+00
		LIN-OPF	LP	6.510e+06	3.91	0.023	0.008	0.102	149.71	14.46	362.42	2.2e+01
		LOLIN-OPF	LP	7.315e+06	−7.97	0.019	0.007	0.078	89.17	1.83	21.31	1.9e+02
		DCPLL	QCP	6.794e+06	−0.28	n.p.	n.p.	n.p.	n.p.	n.p.	n.p.	1.6e+01
		QCWR	QCP	6.641e+06	1.98	n.c.	n.c.	n.c.	n.c.	n.c.	n.c.	7.5e+02
8	case3120sp_k_sad	AC-OPF	NLP	2.176e+06	–	–	–	–	–	–	–	6.9e+00
		DC-OPF	LP	2.252e+06	−3.53	n.p.	n.p.	n.p.	n.p.	n.p.	n.p.	9.4e−01
		LIN-OPF	LP	2.160e+06	0.71	0.004	0.001	0.014	1.31	0.12	2.74	7.4e+00
		LINLOLIN-OPF	LP	n.s.								
		DCPLL	QCP	n.s.								
		QCWR	QCP	2.145e+06	1.41	0.003	0.001	0.033	1.15	0.24	2.49	6.3e+01
9	case2383wp_k_api	AC-OPF	NLP	2.791e+05	–	–	–	–	–	–	–	2.5e+00
		DC-OPF	LP	2.791e+05	0.00	n.p.	n.p.	n.p.	n.p.	n.p.	n.p.	1.7e−01
		LIN-OPF	LP	2.791e+05	0.00	0.002	0.001	0.008	1.49	0.11	1.03	1.8e+00
		LINLOLIN-OPF	LP	2.791e+05	−0.00	0.001	0.001	0.010	3.62	0.22	2.35	3.2e+01
		DCPLL	QCP	2.791e+05	0.00	n.p.	n.p.	n.p.	n.p.	n.p.	n.p.	8.2e−01
		QCWR	QCP	2.791e+05	0.00	0.010	0.005	0.025	15.98	0.71	10.42	1.1e+01
10	case2737sop_k_api	AC-OPF	NLP	4.028e+05	–	–	–	–	–	–	–	4.1e+00
		DC-OPF	LP	3.777e+05	6.24	n.p.	n.p.	n.p.	n.p.	n.p.	n.p.	2.5e−01
		LIN-OPF	LP	3.626e+05	9.98	0.003	0.001	0.010	2.51	0.18	4.99	1.2e+00

(*continued on next page*)

Table 2 (*continued*)

#	Testcase	Method	Problem	Objective	ϵ_O	Magnitude Error (p.u.)			Angle Error (°)			Runtime
				($/h)	(%)	ϵ_v	$\epsilon_{\Delta v}$	max$\lvert\epsilon_{\Delta v}\rvert$	ϵ_θ	$\epsilon_{\Delta\theta}$	max$\lvert\epsilon_{\Delta\theta}\rvert$	(sec)
		LINLOLIN-OPF	LP	4.697e+05	−16.59	0.003	0.001	0.009	3.50	0.21	3.22	1.8e+01
		DCPLL	QCP	4.062e+05	−0.83	n.p.	n.p.	n.p.	n.p.	n.p.	n.p.	1.7e+00
		QCWR	QCP	3.626e+05	9.99	0.002	0.001	0.017	1.60	0.37	3.39	3.7e+01

sufficiently large to approximate the real (practical) range of the absolute values. Too large values might result in weak relaxations leading to branching the problem and hence to an increased computation time.

4. Benchmark study

In this section we aim to show the performance of our proposed OPF methods compared to the nonlinear AC-OPF, the DC-OPF, and to existing approximation and relaxation OPF methods. In particular, we chose the quadratically-constrained (QC) OPF relaxation from [32] and the lossy DC-OPF approximation from [18]. We test our methods based on testcases from MATPOWER [31] and from the benchmark library PGlib [33].

4.1. Implementation

The hardware environment on which our algorithms run is equipped with an Intel Core i7-6600 processor. We implemented the suggested OPF methods within the MATPOWER framework [31] and use the GUROBI [34] solver parametrized with the barrier solver on four cores for solving our methods. The DC-OPF is also solved with GUROBI and with same solver settings. For all other methods, we use the interior point solver IPOPT [35] with the integrated linear system solver MUMPS [36]. The approximation and relaxation methods are solved with PowerModels.jl [37], from which we also adopt the names DCPLL for the lossy DC-OPF approximation and QCWR for QC-OPF relaxation. Both methods are formulated as QC programming (QCP) problems. We set the optimality tolerance for all solvers to 1e−6.

4.2. Error metrics

4.2.1. Voltage errors

We compare the voltage angles and magnitudes ($\boldsymbol{x}_s = \theta, \boldsymbol{v}$) of the approximated OPF solutions with those from the exact power flow (PF) solutions ($\boldsymbol{x}_{pf} = \theta_{pf}, \boldsymbol{v}_{pf}$). For the comparison, we set the PV buses in the PF solution according to the OPF solution and compute the root mean square (RMS) errors ϵ_{x_s} on the nodal angle ($x_s = \theta$) and magnitudes deviations ($x_s = v$)

$$\epsilon_{x_s} = \sqrt{\frac{(\boldsymbol{x}_{pf} - \boldsymbol{x}_s)^T(\boldsymbol{x}_{pf} - \boldsymbol{x}_s)}{n_b}}. \tag{34}$$

Since the nodal errors propagate through the system, we are not able to identify the individual errors from the OPF approximations. The approximation error (ϵ_{y_s}) can be better captured by using the angular ($y_s = \Delta\theta$) and magnitude ($y_s = \Delta v$) differences along the lines and is defined as

$$\epsilon_{y_s} = \sqrt{\frac{(\boldsymbol{y}_{pf} - \boldsymbol{y}_s)^T(\boldsymbol{y}_{pf} - \boldsymbol{y}_s)}{n_l}}. \tag{35}$$

4.2.2. Objective value error

We also define the objective value error between the AC-OPF solution and the approximated solutions. It is defined as

$$\epsilon_O = \frac{f_{AC} - f_z}{f_{AC}}, \tag{36}$$

where f_{AC} is the objective value of the AC-OPF problem and f_z is the objective value of the approximated problem z.

4.3. OPF comparison

The comparison is performed on different test cases ranging from different grid topologies (meshed, radial), voltage levels (distribution, transmission systems), grid sizes, different loading conditions (typical, active power increase (api) conditions), and different operating conditions (small angular deviations (sad)). Table 2 shows the OPF results for the performed test cases and different approximation approaches in terms of objective values, objective value errors, voltage errors, and computation times. The label 'n.p.' indicates that it is not possible to generate a PF solution for the DC-OPF and DCPLL-OPF, while 'n.c.' means that the PF does not converge. The label 'n.s.' indicates that no solution is found. In order to study the impact of negative LMPs on the active power balance, we always check in the AC-OPF solution on negative LMPs. If some exist (mainly in the api test cases), then we run the LINLOLIN-OPF instead of the LOLIN-OPF.

4.3.1. Voltage angle and magnitude error results

First, we aim to analyze the accuracy of our methods. As an example of results, Fig. 6a and b show the angles and magnitudes for the LOLIN-OPF method and for the PF program for the IEEE 118 test grid. Although there is a small deviation in voltage angles, it can be observed that the curves match well. The angle offset can be explained by the fact that our OPF method overestimates the losses at the slack bus, so that this error propagates through the system.

We show the angle and magnitude errors for all other test grids in Table 2. It can be observed that for our suggested methods a feasible PF solution exists, while for the QCWR relaxation for test # 7 the power flow does not converge.

Taking a closer look on the voltage magnitude errors, the MIP-OPF introduces the lowest. This is due to the fact that the MIP-OPF also considers the reactive power losses in the power flow approximation, while this is not the case for the LOLIN-OPF and LIN-OPF.

We observe higher angle errors for the LIN-OPF method, which can be explained that the LIN-OPF version translates the underestimated active power generation setpoints to higher errors in voltage angles. Note that the DC-OPF solution would also generate such error.

4.3.2. Optimality results

Another fact that needs to be discussed is the optimality of our suggested OPF methods. Table 2 lists the objective value errors (ϵ_O) of the analyzed methods. For the typical transmission test cases (#1, 2, 3, 6, 7), we observe at maximum 3.9% for the LIN-OPF, −1.59% for the LINLOLIN-OPF, and −0.92% for LOLIN-OPF. Note that we exclude the LOLIN-OPF result for case #7, since our approach cannot consider negative resistances that correspond to an additional power feed-in. The negative values indicate that the associated methods overestimate the power losses in the grid to some extent. On average, the DC-OPF errors are higher than others. The DC-OPF and LIN-OPF solutions result almost in the same values and have lower objective values compared to

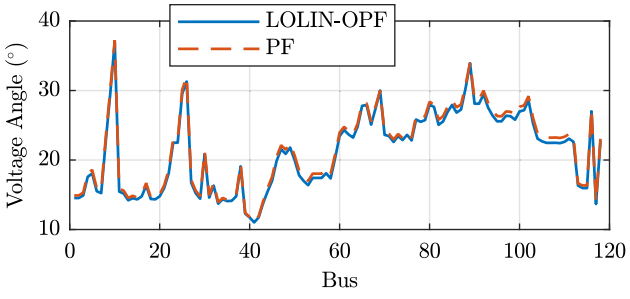

(a) Voltage angle comparison

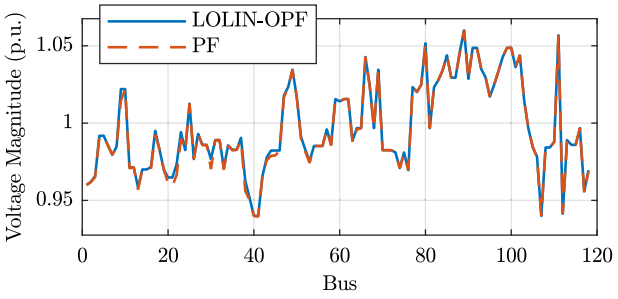

(b) Voltage magnitude comparison

Fig. 6. LOLIN-OPF voltage magnitude and angle comparison with the power flow solution (PF) for the IEEE118 test grid.

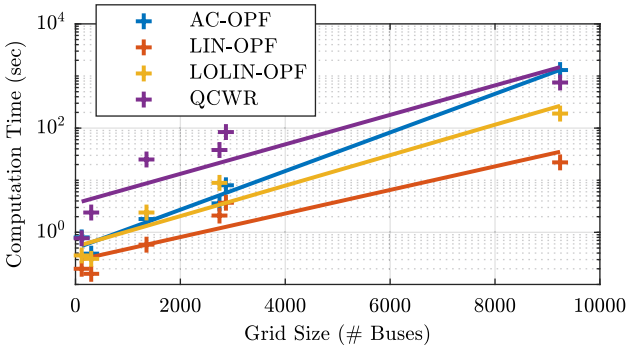

Fig. 7. Computation time comparison between LOLIN-OPF, LIN-OPF, QCWR, and nonlinear AC-OPF and their corresponding lin-log regressions.

the nonlinear OPF solution. This is due to the fact that these methods do not incorporate power losses. In contrast to the DC-OPF, the LIN-OPF also includes a voltage projection. The errors introduced by MIP-OPF and LOLIN-OPF are almost identical.

The objective value errors for the distribution grid test cases #4, 5 are reasonable for the LOLIN-OPF (−5%, −0.47%).

For extreme testcases (#8, 9, 10) the objective value errors deviate (LINLOLIN-OPF −16%, LIN-OPF 10%) much more as for the typical test cases. This is due to the fact that a faithful approximation only holds for an given operating interval, in which k_1 and k_2 was selected for. While the LIN-OPF is feasible for all cases, the DCPLL-OPF and LINLOLIN-OPF do not converge for test case #8.

On average, the DCPLL and QCWR methods achieve lower objective value errors than our suggested methods in absolute terms. But at the same time it is noteworthy that the QCP problems are more complex problems than solving LP/QP problems.

4.3.3. Complexity results

To assess the computational complexity of our methods, we consider only the typical test cases. We observe that the MIP-OPF does not scale well with respect to the grid size, such that this method is not applicable for large grids. The computation time results of the remaining methods that are in the full OPF domain are shown in Fig. 7.

The lin-log regression of the QCWR method is almost shifted in parallel towards higher computation times in the directions of the LIN-OPF and LOLIN-OPF. This means that on average we achieve an improvement in computation time with the LIN-OPF method of one order of magnitude with respect to the QCWR relaxation. The LIN-OPF is almost five times faster than the LOLIN-OPF. Compared to the nonlinear AC-OPF the computation times of the LIN-OPF and LOLIN-OPF are much lower for larger grid sizes. Hence, it can be anticipated that this difference is even more pronounced for multi-period problems, where the grid size multiplies with the planning horizon.

5. Conclusion

In this paper we presented novel tractable OPF methods that work in the full decision domain of active/reactive power and voltage magnitudes/angles. We linearly approximate the power flow over a broader operating range enabling us to solve the problem in a single shot optimization. Our OPF methods can be used by efficient off-the-shelf LP/QP solvers. The obtained accuracy in terms of voltage magnitudes and angles is reasonable and we achieve near-optimal solutions for typical test scenarios. Our methods reduce the computational complexity compared to the nonlinear AC-OPF. For heavily loaded test systems, our methods still find feasible power flow solutions, but result in higher errors in terms of voltage approximation and optimality. This indicates that there exists an operating interval limit, at which only a faithful approximation holds. In order to reduce these errors a future research direction would be to find a more appropriate loss parametrization around the operating point of a specific load case.

Acknowledgment

This project is carried out in the frame of the Swiss Centre for Competence in Energy Research on the Future Swiss Electrical Infrastructure (SCCER-FURIES) with the financial support of the Swiss Commission for Technology and Innovation (CTI – SCCER program).

References

[1] Low SH. Convex relaxation of optimal power flow – part i: formulations and equivalence. IEEE Trans Control Netw Syst 2014;1(1):15–27. https://doi.org/10.1109/TCNS.2014.2309732.
[2] Molzahn DK, Hiskens IA. Moment-based relaxation of the optimal power flow problem. 2014 Power systems computation conference 2014. p. 1–7. https://doi.org/10.1109/PSCC.2014.7038397.
[3] Alguacil N, Motto AL, Conejo AJ. Transmission expansion planning: a mixed-integer LP approach. IEEE Trans Power Syst 2003;18(3):1070–7. https://doi.org/10.1109/TPWRS.2003.814891.
[4] de la Torre S, Conejo AJ, Contreras J. Transmission expansion planning in electricity markets. IEEE Trans Power Syst 2008;23(1):238–48. https://doi.org/10.1109/TPWRS.2007.913717.
[5] Taylor JA, Hover FS. Linear relaxations for transmission system planning. IEEE Trans Power Syst 2011;26(4):2533–8. https://doi.org/10.1109/TPWRS.2011.2145395.
[6] Murillo-Sanchez CE, Zimmerman RD, Lindsay Anderson C, Thomas RJ. Secure planning and operations of systems with stochastic sources, energy storage, and active demand. IEEE Trans Smart Grid 2013;4(4):2220–9. https://doi.org/10.1109/TSG.2013.2281001.
[7] Papavasiliou A, Oren SS. Multiarea stochastic unit commitment for high wind penetration in a transmission constrained network. Oper Res 2013;61(3):578–92. https://doi.org/10.1287/opre.2013.1174.
[8] Amini MH, Bahrami S, Kamyab F, Mishra S, Jaddivada R, Boroojeni K, et al. Decomposition methods for distributed optimal power flow: panorama and case studies of the dc model. In: Zobaa AF, Aleem SHA, Abdelaziz AY, editors. Classical and recent aspects of power system optimization Academic Press; 2018. p. 137–55. https://doi.org/10.1016/B978-0-12-812441-3.00006-9 [chapter 6].
[9] Granville S. Optimal reactive dispatch through interior point methods. IEEE Trans Power Syst 1994;9(1):136–46. https://doi.org/10.1109/59.317548.
[10] Schenk O, Gärtner K. Solving unsymmetric sparse systems of linear equations with PARDISO. Future Gener Comput Syst 2004;20(3):475–87. https://doi.org/10.1016/J.FUTURE.2003.07.011.
[11] Wang H, Murillo-Sanchez CE, Zimmerman RD, Thomas RJ. On computational issues

of market-based optimal power flow. IEEE Trans Power Syst 2007;22(3):1185–93. https://doi.org/10.1109/TPWRS.2007.901301.
[12] Kourounis D, Fuchs A, Schenk O. Towards the next generation of multiperiod optimal power flow solvers. IEEE Trans Power Syst 2018:1. https://doi.org/10.1109/TPWRS.2017.2789187.
[13] Baringo L, Baringo A. A stochastic adaptive robust optimization approach for the generation and transmission expansion planning. IEEE Trans Power Syst 2017;8950(c):1. https://doi.org/10.1109/TPWRS.2017.2713486.
[14] Amjady N, Dehghan S, Attarha A, Conejo AJ. Adaptive robust network-constrained AC unit commitment. IEEE Trans Power Syst 2017;32(1):672–83. https://doi.org/10.1109/TPWRS.2016.2562141.
[15] Kirschen D, Van Meeteren H. MW/voltage control in a linear programming based optimal power flow. IEEE Trans Power Syst 1988;3(2):481–9. https://doi.org/10.1109/59.192899.
[16] Alsaç O, Bright J, Prais M, Stott B. Further developments in LP-based optimal power flow. IEEE Trans Power Syst 1990;5(3):697–711. https://doi.org/10.1109/59.65896.
[17] Olofsson M, Andersson G, Söder L. Linear programming based optimal power flow using second order sensitivities. IEEE Trans Power Syst 1995;10(3):1691–7.
[18] Coffrin C, Van Hentenryck P, Bent R. Approximating line losses and apparent power in AC power flow linearizations. IEEE power and energy society general meeting 2012. p. 1–8. https://doi.org/10.1109/PESGM.2012.6345342.
[19] Coffrin C, Hentenryck PV. A linear-programming approximation of AC power flows. INFORMS J Comput 2014;26(4):718–34. https://doi.org/10.1287/ijoc.2014.0594.
[20] Koster ACA, Lemkens S. Designing AC power grids using integer linear programming. Netw Optimiz 2011;6701:478–83. https://doi.org/10.1007/978-3-642-21527-8_52.
[21] Bolognani S, Zampieri S. On the existence and linear approximation of the power flow solution in power distribution networks. IEEE Trans Power Syst 2016;31(1):163–72. https://doi.org/10.1109/TPWRS.2015.2395452.
[22] Motto AL, Galiana ED. Network-constrained multiperiod auction for a pool-based electricity market. IEEE Power Eng Rev 2002;22(6):58. https://doi.org/10.1109/MPER.2002.4312289.
[23] Yang Z, Zhong H, Bose A, Zheng T, Xia Q, Kang C. A linearized OPF model with reactive power and voltage magnitude: a pathway to improve the MW-only DC OPF. IEEE Trans Power Syst 2018;33(2):1734–45. https://doi.org/10.1109/TPWRS.2017.2718551.
[24] Zhang H, Vittal V, Heydt GT, Quintero J. A relaxed AC optimal power flow model based on a Taylor series. 2013 IEEE innovative smart grid technologies-Asia (ISGT Asia) 2013. p. 1–5. https://doi.org/10.1109/ISGT-Asia.2013.6698739.
[25] Mhanna S, Verbič G, Chapman AC. Tight LP approximations for the optimal power flow problem. 19th power systems computation conference, PSCC 2016. https://doi.org/10.1109/PSCC.2016.7540937.
[26] Castillo A, Lipka P, Watson J-P, Oren SS, O'Neill RP. A successive linear programming approach to solving the IV-ACOPF. IEEE Trans Power Syst 2016;31(4):2752–63. https://doi.org/10.1109/TPWRS.2015.2487042.
[27] Hörsch J, Ronellenfitsch H, Witthaut D, Brown T. Linear optimal power flow using cycle flows. Electr Power Syst Res 2018;158:126–35. https://doi.org/10.1016/j.epsr.2017.12.034.
[28] Martin JA, Hiskens IA. Generalized line loss relaxation in polar voltage coordinates. IEEE Trans Power Syst 2017;32(3):1980–9. https://doi.org/10.1109/TPWRS.2016.2595763.
[29] Stott B, Alsac O. Fast decoupled load flow. IEEE Trans Power Apparatus Syst PAS-93 1974(3):859–69. https://doi.org/10.1109/TPAS.1974.293985.
[30] Garces A. A quadratic approximation for the optimal power flow in power distribution systems. Electr Power Syst Res 2016;130:222–9. https://doi.org/10.1016/j.epsr.2015.09.006.
[31] Zimmerman RD, Murillo-Sanchez CE, Thomas RJ. MATPOWER: steady-state operations, planning, and analysis tools for power systems research and education. IEEE Trans Power Syst 2011;26(1):12–9. https://doi.org/10.1109/TPWRS.2010.2051168.
[32] Hijazi H, Coffrin C, Hentenryck PV. Convex quadratic relaxations for mixed-integer nonlinear programs in power systems. Math Program Comput 2017;9(3):321–67. https://doi.org/10.1007/s12532-016-0112-z.
[33] The IEEE PES task force on benchmarks for validation of emerging power system algorithms. PGLib optimal power flow benchmarks. < https://github.com/power-grid-lib/pglib-opf > [accessed: 2018-04-01].
[34] Gurobi Optimization, Inc.. Gurobi optimizer reference manual; 2016. < http://www.gurobi.com > .
[35] Wächter A, Biegler LT. On the implementation of an interior-point filter line-search algorithm for large-scale nonlinear programming. Math Program 2006;106(1):25–57. https://doi.org/10.1007/s10107-004-0559-y.
[36] Amestoy PR, Duff IS, L'Excellent J-Y, Koster J. A fully asynchronous multifrontal solver using distributed dynamic scheduling. SIAM J Matrix Anal Appl 2001;23(1):15–41. https://doi.org/10.1137/S0895479899358194.
[37] Coffrin C, Bent R, Sundar K, Ng Y, Lubin M. Powermodels. JL: an open-source framework for exploring power flow formulations. 2018 power systems computation conference (PSCC) 2018. p. 1–8. https://doi.org/10.23919/PSCC.2018.8442948.
[38] C. Josz, S. Fliscounakis, J. Maeght, P. Panciatici, AC power flow data in MATPOWER and QCQP format: iTesla, RTE snapshots, and PEGASE, 2016, pp. 1–7. Available from: 1603.01533.
[39] Fortenbacher P, Zellner M, Andersson G. Optimal sizing and placement of distributed storage in low voltage networks. 2016 Power systems computation conference (PSCC) IEEE; 2016. p. 1–7. https://doi.org/10.1109/PSCC.2016.7540850.